PAPER

Fast generation of spin squeezing via resonant spin-boson coupling

View the article online for updates and enhancements.

Quantum Science and Technology

PAPER

Fast generation of spin squeezing via resonant spin-boson coupling

Diego Barberena[1,4,*] , Sean R Muleady[1,4] , John J Bollinger[2] , Robert J Lewis-Swan[3] and Ana Maria Rey[1]

[1] JILA, NIST, Department of Physics, University of Colorado, Boulder, CO 80309, United States of America
[2] National Institute of Standards and Technology, Boulder, CO 80305, United States of America
[3] Homer L. Dodge Department of Physics and Astronomy, The University of Oklahoma, Norman, OK 73019, United States of America
[4] These two authors contributed equally.
* Author to whom any correspondence should be addressed.

E-mail: diba2060@colorado.edu

Abstract

We propose protocols for the creation of useful entangled states in a system of spins collectively coupled to a bosonic mode, directly applicable to trapped-ion and cavity QED setups. The protocols use coherent manipulations of the resonant spin-boson interactions naturally arising in these systems to prepare spin squeezed states exponentially fast in time. The resonance condition harnesses the full spin-boson coupling and thus avoids the slower timescales when operating in the off-resonance regime. We demonstrate the robustness of the protocols by analyzing the effects of natural sources of decoherence in these systems and show their advantage compared to more standard slower approaches where entanglement is generated with off-resonant spin-boson interactions.

1. Introduction

Spin squeezed states [1–4] are a robust example of simple entangled states that can overcome the so called standard quantum limit (SQL) or fundamental noise floor achievable with N uncorrelated particles. Consequently, they have become an important resource for quantum-enhanced sensing and their preparation is a target of intensive research in many different state-of-the-art quantum platforms [5–14]. While spin squeezing can be generated by diverse mechanisms, a common dynamical approach is one-axis twisting (OAT) [1], involving an infinite range Ising interaction between a collection of two level systems. Many schemes to engineer OAT make use of long-range interactions realized in atom-boson platforms, which typically operate in a far-detuned regime where the bosonic degree of freedom only mediates interactions between the spins [7, 12, 15]. Consequently, the generated spin–spin interactions are slow compared to the original atom-boson coupling, making any generated squeezing susceptible to decoherence.

Here, we propose to generate spin squeezing through a scheme that *resonantly* couples spins to a bosonic degree of freedom and fully leverages the available atom-boson coupling. This is achieved by implementing various spin-boson models that can be concatenated together to prepare a desired final quantum state. We describe a pair of simple protocols to create metrologically useful entanglement exponentially fast, in line with existing proposals and implementations in spin models [1, 15–17], but with the beneficial short timescales associated with the resonant interactions. Furthermore, we characterize the fundamentally achievable phase sensitivity of the protocols as a function of particle number.

In the simplest case, we predict that states with noise variance squeezed by a factor of $\sim N^{-1/2}$ below the SQL can be realized, but we also show that this can be enhanced to near the Heisenberg limit ($\sim N^{-1}$) [18, 19] by using a time-reversal readout protocol to access entanglement beyond the paradigm of squeezed states. We complement the analysis by assessing the performance of both protocols in the presence of decoherence and determine under what conditions they may outperform standard OAT.

Our results are relevant for a range of platforms that use spin-boson couplings or pairs of collective spin ensembles for entanglement generation [20]. Here, we explicitly demonstrate their utility in 2D arrays of trapped ions and cavity QED systems [12], where previous attempts at spin squeezing using OAT had been constrained by decoherence.

2. Model

Our proposal utilizes the TC [21] and anti-TC (ATC) Hamiltonians for N spin-1/2 particles,

$$\hat{H}_{\text{TC}} = -\frac{iG}{\sqrt{N}}\left(\hat{a}\hat{S}^+ - \hat{a}^\dagger\hat{S}^-\right), \tag{1}$$

$$\hat{H}_{\text{ATC}} = -\frac{iG}{\sqrt{N}}\left(\hat{a}^\dagger\hat{S}^+ - \hat{a}\hat{S}^-\right), \tag{2}$$

where $\hat{S}_\alpha = 1/2\sum_{j=1}^N \hat{\sigma}_j^\alpha$ are collective spin operators for $\alpha = x, y, z$, the $\hat{\sigma}_j^\alpha$ are Pauli matrices acting on the jth spin, and G is a coupling constant whose value and N scaling depend on the specific experimental platform. The bosonic degree of freedom is described by the annihilation (creation) operator, $\hat{a}$ ($\hat{a}^\dagger$), while $\hat{S}^\pm$ are spin raising (lowering) operators, traditionally defined as $\hat{S}^\pm = \hat{S}_x \pm i\hat{S}_y$.

To elucidate the utility of the TC and ATC Hamiltonians for rapid entanglement generation and manipulation, we consider a scenario where an initial spin state is polarized along $+z$ on the collective Bloch sphere. When N is very large, the collective spin operators can be represented by an auxiliary bosonic system with annihilation operator $\hat{b}$, using the lowest-order approximation in a Holstein–Primakoff transformation [22]

$$\hat{S}^+ \approx i\sqrt{N}\hat{b}, \qquad \hat{S}^- \approx -i\sqrt{N}\hat{b}^\dagger, \qquad \hat{S}_z = N/2 - \hat{b}^\dagger\hat{b} \tag{3}$$

such that the coherent spin state pointing along $+z$ corresponds to the bosonic vacuum, $|(N/2)_z\rangle = |0\rangle_b$. The TC and ATC spin-boson models in equations (1) and (2) then give rise to bosonic two-mode squeezing and beam splitter Hamiltonians

$$\hat{H}_{\text{TMS}} = G\left(\hat{a}\hat{b} + \hat{a}^\dagger\hat{b}^\dagger\right), \qquad \hat{H}_{\text{BS}} = G\left(\hat{a}^\dagger\hat{b} + \hat{a}\hat{b}^\dagger\right), \tag{4}$$

respectively. In terms of the hybrid modes $\hat{c}_\pm = (\hat{a} \pm \hat{b})/\sqrt{2}$ and their associated quadratures $\hat{x}_\pm = (\hat{c}_\pm + \hat{c}_\pm^\dagger)/\sqrt{2}$, $\hat{p}_\pm = (\hat{c}_\pm - \hat{c}_\pm^\dagger)/(i\sqrt{2})$, the dynamics created by $\hat{H}_{\text{TMS}}$ and $\hat{H}_{\text{BS}}$ decouple. These modes appear in $\hat{H}_{\text{TMS}}$ in the form of a classically unstable inverted parabolic potential ($p_\pm^2 - \hat{x}_\pm^2$), which amplifies quantum fluctuations in a coherent fashion (see figure 1(b)). Conversely, $\hat{H}_{\text{BS}}$ has the form of a stable parabolic potential ($p_\pm^2 + \hat{x}_\pm^2$), which facilitates the perfect transfer of quantum states between spin and boson degrees of freedom. For later convenience, we also define the canonically conjugate quadrature operators $\hat{x}_a = (\hat{a} + \hat{a}^\dagger)/\sqrt{2}$ and $\hat{p}_a = -i(\hat{a} - \hat{a}^\dagger)/\sqrt{2}$.

2.1. Squeeze and transfer protocol (SnT)
Using the TMS and BS Hamiltonians, we describe a protocol that we refer to as SnT (*squeeze and transfer*), which creates squeezing in the spin and boson subsystems simultaneously (see figure 1(b)). We begin by (1) preparing the spins polarized along $+z$ and the bosons in vacuum $|\psi(0)\rangle = |(N/2)_z\rangle \otimes |0\rangle$, and let $\hat{H}_{\text{TC}}$ act so that $\hat{H}_{\text{TMS}}$ is active. (2) We let the system evolve in this configuration for a time T_{sq} and then (3) quench $\hat{H}_{\text{TC}} \to -\hat{H}_{\text{ATC}}$ so that now the BS interaction $\hat{H}_{\text{BS}}$ acts for a time T_{tr}. These steps are illustrated in figure 1(b) using phase space representations of the spin and boson states at different stages of the protocol.

The initial state of the system is shown in figure 1(b) as two independent isotropic Gaussian distributions in phase space. According to the effective description of $\hat{H}_{\text{TMS}}$, squeezing is created independently in the hybrid modes (x_+, p_+) and (x_-, p_-). The final BS step, when run for a time $GT_{\text{tr}} = \pi/4$, decouples these hybrid modes such that spins and bosons end up independently squeezed. For this configuration, the resultant spin squeezing is quantified by [23]

$$\xi^2 \equiv \min_\theta N\frac{\left\langle\left(\Delta\hat{S}_\theta\right)^2\right\rangle}{\left\langle\hat{S}_z\right\rangle^2} \approx e^{-2GT_{\text{sq}}}, \tag{5}$$

where the variance of the transverse spin $\hat{S}_\theta = \cos(\theta)\hat{S}_x + \sin(\theta)\hat{S}_y$ is minimized over all angles θ, and all expectation values are calculated at the end of the protocol. When $\xi^2 < 1$ we say the state is spin squeezed,
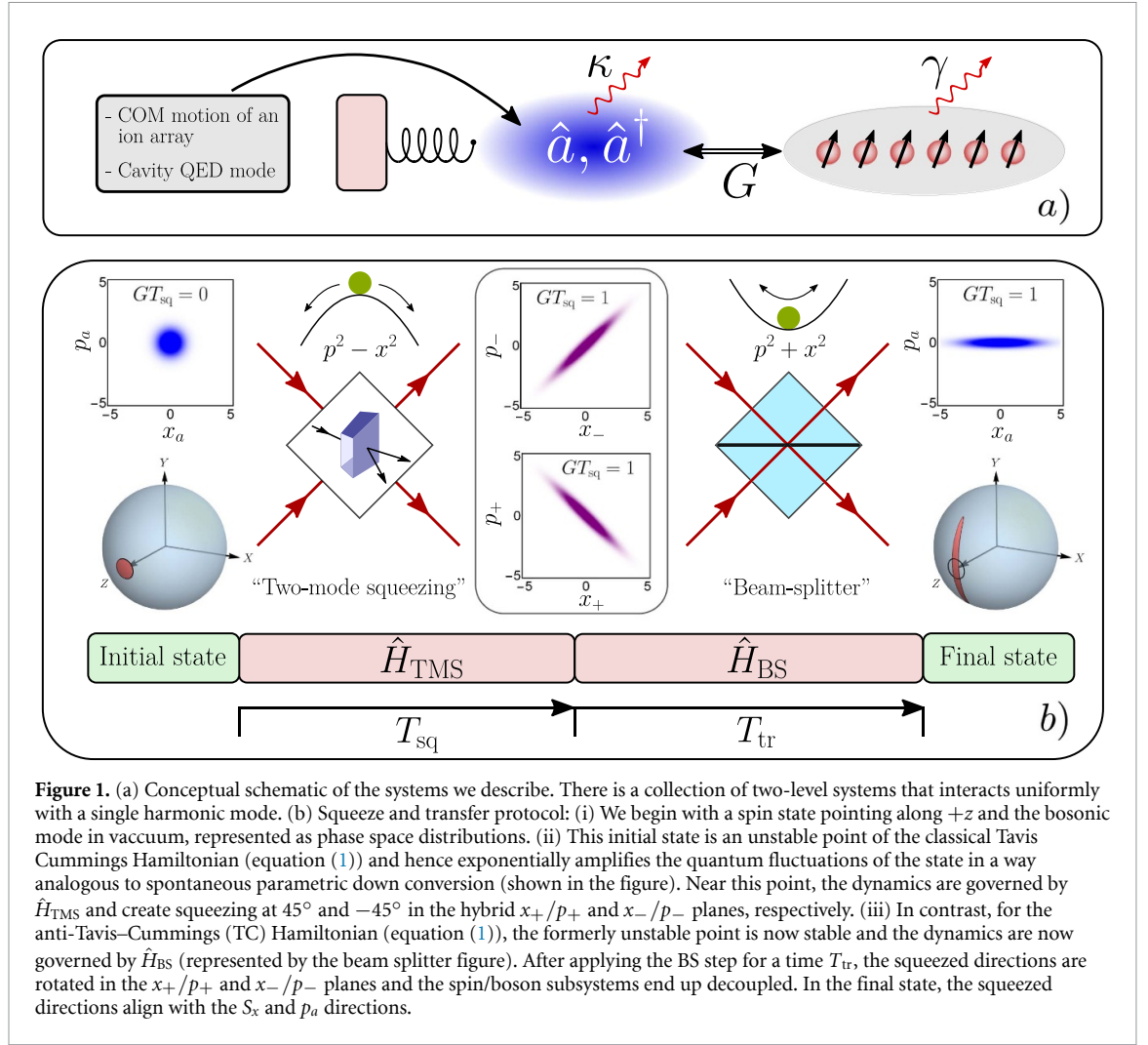
Figure 1. (a) Conceptual schematic of the systems we describe. There is a collection of two-level systems that interacts uniformly with a single harmonic mode. (b) Squeeze and transfer protocol: (i) We begin with a spin state pointing along $+z$ and the bosonic mode in vaccum, represented as phase space distributions. (ii) This initial state is an unstable point of the classical Tavis Cummings Hamiltonian (equation (1)) and hence exponentially amplifies the quantum fluctuations of the state in a way analogous to spontaneous parametric down conversion (shown in the figure). Near this point, the dynamics are governed by $\hat{H}_{\mathrm{TMS}}$ and create squeezing at 45° and −45° in the hybrid x_+/p_+ and x_-/p_- planes, respectively. (iii) In contrast, for the anti-Tavis–Cummings (TC) Hamiltonian (equation (1)), the formerly unstable point is now stable and the dynamics are now governed by $\hat{H}_{\mathrm{BS}}$ (represented by the beam splitter figure). After applying the BS step for a time T_{tr}, the squeezed directions are rotated in the x_+/p_+ and x_-/p_- planes and the spin/boson subsystems end up decoupled. In the final state, the squeezed directions align with the S_x and p_a directions.

which also indicates the presence of entanglement [2]. The right hand side of equation (5) is obtained in the limit of large N. Simultaneously, we find that noise in the boson quadrature $\hat{p}_a$ is similarly squeezed by an amount $e^{-2GT_{\mathrm{sq}}}$ [24]. Under ideal conditions, this exponential growth will only be constrained by curvature effects arising from finite N, which are caused by higher order corrections in the Holstein–Primakoff expansion of equation (3) and set in when the initial state becomes moderately depleted. This generically prevents the squeezing from reaching the Heisenberg limit ($\xi_{\mathrm{H}}^2 = 1/N$).

2.2. Time-reversal

The limitations arising from curvature can typically be countered by applying the entangling interaction ($\hat{H}_{\mathrm{TMS}}$ in our case) within a time-reversal scheme [9, 25–33]. This protocol begins with the same initial state $|N/2_z\rangle \otimes |0\rangle_b$ and proceeds by letting the TMS interaction act for a time T_1. The resulting spin-boson entangled state (same as in figure 1(b), middle column) constitutes our quantum-enhanced metrological resource, and can be directly perturbed by the infinitesimal rotation $\exp(-i\phi\hat{S}_x)$ that we seek to characterize[5]. The readout process then consists of applying the TMS Hamiltonian an amount of time T_2 (typically taken to be equal to T_1), but with the opposite sign ($g \to -g$), and a final measurement of $\hat{S}_\theta$ for an appropriately selected θ.

The choice of $\hat{S}_\theta$ as a measurement observable defines the sensitivity to small rotations

$$\delta\phi^2 \equiv \frac{\left\langle \left(\Delta \hat{S}_\theta\right)^2 \right\rangle}{|\partial_\phi \left\langle \hat{S}_\theta \right\rangle|^2} \approx \frac{1}{N\cosh\left(GT/2\right)^2}, \tag{6}$$

---

[5] The axis of rotation can be chosen to be along any direction in the XY plane for a Bloch vector pointing along $+z$. Sensitivity with respect to more general axes can be attained by applying single particle rotations before and after the perturbation.

where we minimize over θ, generically assuming $\phi \to 0$, and the expectation values and variances are calculated at the end of the protocol. To obtain the right-hand side of equation (6), we set $T_1 = T_2 = T/2$ (T is total protocol time) and assume $N \to \infty$ [34]. Once again, the metrological enhancement over the SQL ($\delta\phi^2_{\mathrm{SQL}} = 1/N$) improves exponentially with time. In time-reversal schemes, this metrological enhancement arises from an amplification of the signal ($\partial_\phi \langle \hat{S}_\theta \rangle$) as the total protocol time T grows, while the noise $[(\Delta \hat{S}_\theta)^2]$ at the end of the protocol is independent of T and about the size of quantum projection noise. As in SnT, the exponentially fast enhancement is a consequence of operating the system at the classically unstable point described by $\hat{H}_{\mathrm{TMS}}$. This is a generic feature that can be exploited to implement efficient time-reversal in a diverse set of platforms [9, 25–33].

An important feature of this time-reversal protocol is that there is spin-boson entanglement during the signal acquisition step ($e^{-i\phi \hat{S}_x}$). In contrast, SnT only prepares the metrological resource, i.e. a spin squeezed state decoupled from the bosons, after which signal acquisition would commence, commonly via a Ramsey protocol. This distinction is of practical importance in the presence of decoherence: in time-reversal, both boson and spin coherence need to be maintained throughout signal acquisition, which is typically the longest part of the protocol. In SnT, only spin coherence is relevant during this stage since spins and bosons are decoupled.

3. Trapped ion implementation

In trapped ion crystals, the TC and ATC models can be indirectly generated by operating at different parameter regimes of the Dicke model [35–42], written in a spin rotated basis as

$$\hat{H}^{\mathrm{ion}}_{\mathrm{Dicke}} = \delta \hat{a}^\dagger \hat{a} + \Omega \hat{S}_x + \frac{2g_{\mathrm{ion}}}{\sqrt{N}} \left(\hat{a} + \hat{a}^\dagger \right) \hat{S}_z. \tag{7}$$

The spin degree of freedom is encoded in the ion internal levels, while the boson corresponds to a motional mode of the ion array, typically a center of mass mode. The Hamiltonian in equation (7) can be realized, for example, in the Penning trap implementation described in [12, 32, 43], where the transverse center of mass motional mode of a planar 2D crystal of $N \approx 150$ $^9\mathrm{Be}^+$ ions is coupled to the two $2s\,^2S_{1/2}$ valence electron spin states using optical dipole forces (ODF), engineered through a pair of detuned lasers. The electronic states are split by a large magnetic field present in the experiment and can be coherently manipulated using microwaves, which determine the sign and strength of the transverse field $\Omega \hat{S}_x$. The effective oscillator frequency δ is controlled by the difference between the natural oscillation frequency of the center of mass mode and the detuning between the ODF lasers, while the size and sign of the N-independent coupling g_{ion} is controlled by their intensity and relative phase, respectively. The dynamics of this system are then described by equation (7) in a frame where the bosons are rotating at the beatnote frequency of the ODF lasers.
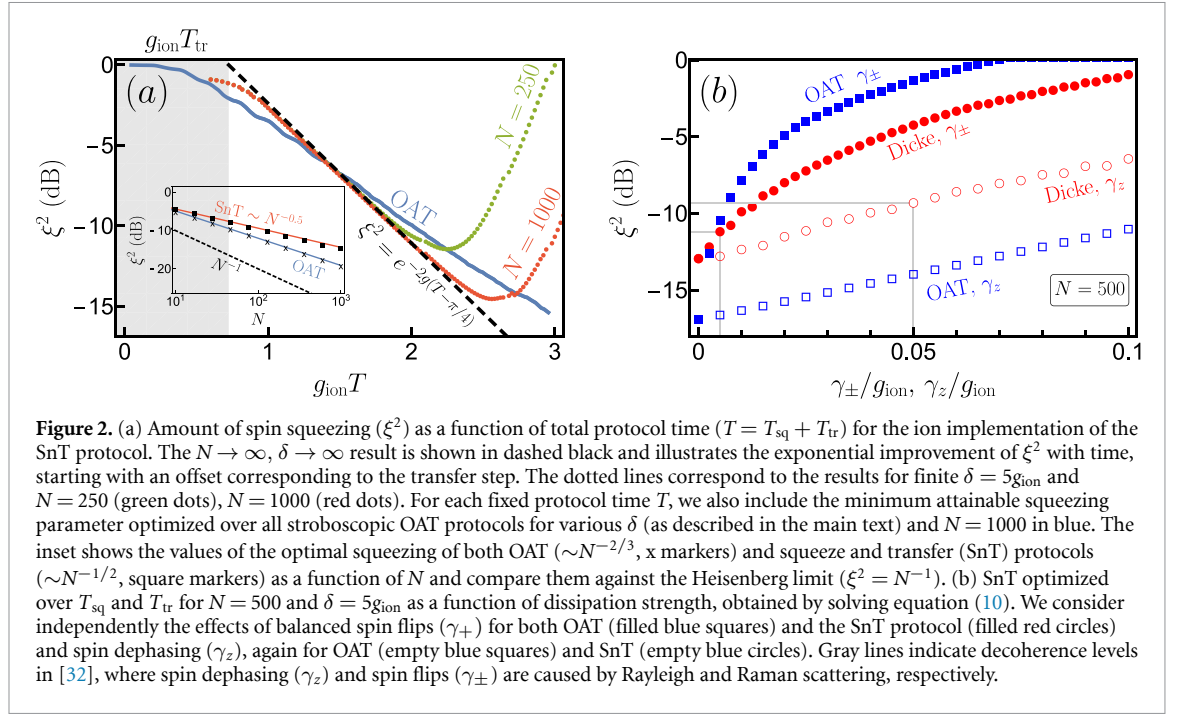
In the interaction picture induced by $\hat{H}_0 = \delta \hat{a}^\dagger \hat{a} + \Omega \hat{S}_x$, the Dicke Hamiltonian equation (7) takes the form

$$\hat{H}^{\mathrm{ion}}_{\mathrm{rot}} = -\frac{ig_{\mathrm{ion}}}{\sqrt{N}} \left(\hat{a} e^{-i\delta t} + \hat{a}^\dagger e^{i\delta t} \right) \left(\hat{S}^+_{\mathrm{ion}} e^{i\Omega t} - \hat{S}^-_{\mathrm{ion}} e^{-i\Omega t} \right), \tag{8}$$

where $\hat{S}^\pm_{\mathrm{ion}} = \hat{S}_y \pm i\hat{S}_z$ are raising and lowering operators along the $+x$ direction. Assuming $\delta \gg g_{\mathrm{ion}}$ and setting $\delta = \Omega$ or $\delta = -\Omega$ we can then apply a rotating wave approximation to recover equation (1) or equation (2), respectively, with $G_{\mathrm{ion}} = g_{\mathrm{ion}}$. Owing to the rotated spin basis, the spins should be initialized along $+x$ instead of $+z$ for step (1) of the protocol.

3.1. Squeeze and transfer (SnT)

The time profile of spin squeezing given by equation (5) for the SnT protocol is only strictly valid in the limit $N \to \infty$, while the trapped ion implementation further requires that $\delta \to \infty$. To benchmark our predictions for finite N and δ, we numerically solve equation (7) for $N = 250, 1000$ and constraining $\delta = 5g_{\mathrm{ion}}$. Given that the result $g_{\mathrm{ion}} T_{\mathrm{tr}} = \pi/4$ also depends on the previous approximations, in our simulations we optimize over T_{tr} for each value of T_{sq} but find that the optimal transfer time remains close to the ideal, with larger deviations occurring at small δ [34]. We show this optimized value of ξ^2 in figure 2(a) and compare it against equation (5). The numerical calculations match the expected exponential squeezing at short times, before slowing and attaining a minimum value due to finite size effects. A systematic analysis of the achievable minimum squeezing with N (see figure 2 inset) reveals a scaling $\xi^2 \sim N^{-1/2}$ that is reached at $g_{\mathrm{ion}} T_{\mathrm{sq}} \sim (\log N)/4$. More sophisticated measurements [12, 18, 19, 44, 45], as well as time-reversal

Figure 2. (a) Amount of spin squeezing (ξ^2) as a function of total protocol time ($T = T_{sq} + T_{tr}$) for the ion implementation of the SnT protocol. The $N \to \infty$, $\delta \to \infty$ result is shown in dashed black and illustrates the exponential improvement of ξ^2 with time, starting with an offset corresponding to the transfer step. The dotted lines correspond to the results for finite $\delta = 5g_{ion}$ and $N = 250$ (green dots), $N = 1000$ (red dots). For each fixed protocol time T, we also include the minimum attainable squeezing parameter optimized over all stroboscopic OAT protocols for various δ (as described in the main text) and $N = 1000$ in blue. The inset shows the values of the optimal squeezing of both OAT ($\sim N^{-2/3}$, x markers) and squeeze and transfer (SnT) protocols ($\sim N^{-1/2}$, square markers) as a function of N and compare them against the Heisenberg limit ($\xi^2 = N^{-1}$). (b) SnT optimized over T_{sq} and T_{tr} for $N = 500$ and $\delta = 5g_{ion}$ as a function of dissipation strength, obtained by solving equation (10). We consider independently the effects of balanced spin flips (γ_+) for both OAT (filled blue squares) and the SnT protocol (filled red circles) and spin dephasing (γ_z), again for OAT (empty blue squares) and SnT (empty blue circles). Gray lines indicate decoherence levels in [32], where spin dephasing (γ_z) and spin flips ($\gamma_\pm$) are caused by Rayleigh and Raman scattering, respectively.

strategies [9, 25–31, 34] (as discussed below), can further improve the sensitivity closer to the Heisenberg limit, though decoherence can impose serious limitations on this [46, 47].

For clarity, we compare our results for SnT against the typical squeezing generated by the OAT model in the trapped ion setting

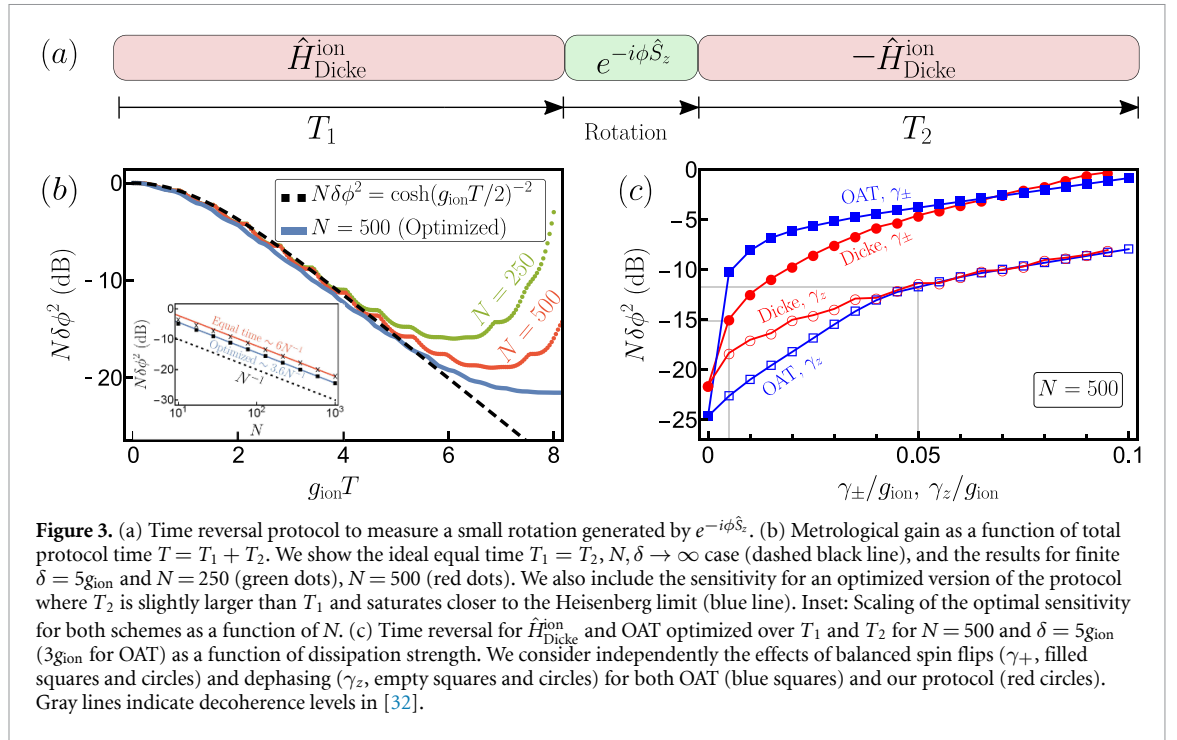$$\hat{H}_{OAT} = -\frac{4g_{ion}^2}{\delta N} \left(\hat{S}_z \right)^2, \tag{9}$$

which arises from equation (7) when $\Omega = 0$. Strictly speaking, OAT only emerges from equation (7) in the large detuning limit $\delta \gg g_{ion}$ where the bosons can be adiabatically eliminated. Nevertheless, the OAT dynamics can still be reached in a stroboscopic protocol which only measures the spins at times $T = 2\pi n/\delta$ with n an integer, when they fully decouple from the bosons [12, 48]. We adopt the latter approach, numerically solving equation (7) for $\Omega = 0$. For fairness we compare to the total protocol time ($T = T_{tr} + T_{sq}$) at fixed values of g_{ion} and $N = 1000$, and optimize the attainable squeezing at stroboscopic times over all tunable parameters, such as δ/g_{ion}, for each time T. While the overall time duration of SnT initially suffers from the fixed T_{tr} offset, this is eventually overwhelmed by the exponentially fast TMS dynamics. If we take into account finite size effects, the absolute squeezing attainable with OAT has a more favourable scaling ($N^{-2/3}$ for OAT vs $N^{-1/2}$ for our protocol, see inset of figure 2(a)), but is attained at progressively longer times $g_{ion}^2 T_{opt}/\delta \sim N^{1/3}$ as the number of particles grows, whereas the time required for our protocol is essentially constant for all experimentally relevant particle numbers ($g_{ion} T_{opt} \sim \log N$).

These shorter time scales can lead to a substantial net gain in spin squeezing in the presence of experimentally relevant decoherence. During the preparation stage, relevant decoherence processes are dephasing and spin flips, with jump operators $\sqrt{\gamma_z}\hat{\sigma}_z^i/2$ and $\sqrt{\gamma_\pm}\hat{\sigma}_i^\pm$, respectively. For simplicity in our following discussion we set $\gamma_+ = \gamma_-$. In the context of trapped ion simulators, e.g. such as [32], these spin decoherence processes are a consequence of the applied ODF, and bosonic decay is not relevant.

In the presence of these decoherence sources, the evolution of the system is governed by the master equation

$$\partial_t \hat{\rho} = -i \left[\delta \hat{a}^\dagger \hat{a} + \Omega(t) \hat{S}_x + \frac{2g_{ion}}{\sqrt{N}} \hat{S}_z \left(\hat{a}^\dagger + \hat{a} \right), \hat{\rho} \right]$$
$$+ \frac{\gamma_z}{4} \sum_{i=1}^{N} \left(\hat{\sigma}_z^i \hat{\rho} \hat{\sigma}_z^i - \hat{\rho} \right) + \frac{\gamma_+}{2} \sum_{i=1}^{N} \left(\hat{\sigma}_x^i \hat{\rho} \hat{\sigma}_x^i + \hat{\sigma}_y^i \hat{\rho} \hat{\sigma}_y^i - 2\hat{\rho} \right), \tag{10}$$

where we consider a time dependent $\Omega(t)$ to take into account the quench from $\Omega \to -\Omega$ necessary to toggle between $\hat{H}_{TMS}$ and $\hat{H}_{BS}$.

Figure 3. (a) Time reversal protocol to measure a small rotation generated by $e^{-i\phi \hat{S}_z}$. (b) Metrological gain as a function of total protocol time $T = T_1 + T_2$. We show the ideal equal time $T_1 = T_2$, $N, \delta \to \infty$ case (dashed black line), and the results for finite $\delta = 5g_{\text{ion}}$ and $N = 250$ (green dots), $N = 500$ (red dots). We also include the sensitivity for an optimized version of the protocol where T_2 is slightly larger than T_1 and saturates closer to the Heisenberg limit (blue line). Inset: Scaling of the optimal sensitivity for both schemes as a function of N. (c) Time reversal for $\hat{H}_{\text{Dicke}}^{\text{ion}}$ and OAT optimized over T_1 and T_2 for $N = 500$ and $\delta = 5g_{\text{ion}}$ ($3g_{\text{ion}}$ for OAT) as a function of dissipation strength. We consider independently the effects of balanced spin flips (γ_+, filled squares and circles) and dephasing (γ_z, empty squares and circles) for both OAT (blue squares) and our protocol (red circles). Gray lines indicate decoherence levels in [32].

To efficiently investigate the impact of spin decoherence for moderate size systems we solve equation (10) using a semiclassical numerical method [49], which has been shown to accurately capture the effects of single-particle dissipation for similar spin-boson models and which we benchmark for equation (7) in [34]. The results are shown in figure 2(b), where we plot the squeezing of SnT as a function of dissipation strength after optimization over T_{sq} and T_{tr}. We find that SnT is substantially more robust than OAT against spin flips but less robust against dephasing. In the latter case, a large fraction of the discrepancy can be accounted for by finite size effects. Using [32] as a state-of-the-art example, typical decoherence rates are $\gamma_z = 610\,\text{s}^{-1} \approx 0.05g_{\text{ion}}$ and $\gamma_+ = 61\,\text{s}^{-1} \approx 0.005g_{\text{ion}}$ ($g_{\text{ion}} = 2\pi \times 2$ kHz, $\Omega \sim 2\pi \times 10$–15 kHz). For this set of parameters, figure 2(b) indicates that dephasing is slightly more relevant than spin flips, with an expected squeezing of about 9 dB (see gray lines in figure 2(b)).

It is important to point out that the current laser configuration used in the Penning trap has been optimized assuming a target Hamiltonian of the form of equation (9), i.e. a Hamiltonian that scales as g_{ion}^2. Nevertheless, as pointed out in recent studies [50], for the case when the Hamiltonian dynamics scales linearly with g_{ion}, as in our resonant approach, it should be possible to use an ODF configuration that features a more favorable scaling of g_{ion}/γ_z and thus a significantly reduced impact from decoherence.

3.2. Time-reversal

In the trapped ion implementation, time reversal of the Hamiltonian in equation (7) requires that $(\delta, \Omega, g_{\text{ion}}) \to -(\delta, \Omega, g_{\text{ion}})$ halfway through the protocol. Furthermore, because of the rotated spin basis in which we are operating, the perturbation that we are trying to characterize is generated by $e^{-i\phi \hat{S}_z}$ (or any axis of rotation in the YZ plane) instead of $e^{-i\phi \hat{S}_x}$ (see figure 3(a)).

As in the case of SnT, the time profile of the sensitivity shown in equation (6) is only valid in the limits $N, \delta \to \infty$, so we numerically test our predictions by solving equation (7) for $N = 250$ and $N = 500$ with $\Omega = \delta = 5g_{\text{ion}}$. The results, shown in figure 3(b), indicate that the metrological enhancement follows the expected $\cosh(g_{\text{ion}}T/2)$ behaviour at short times, but then reaches a minimum that depends on the system size N. In contrast to SnT, this minimum shows Heisenberg scaling ($N\delta\phi^2 \sim N^{-1}$, see figure 3(b) inset). Intriguingly, further enhancement can be obtained by operating with unequal forward and backward interaction times, allowing for an additional gain of up to 3 dB (see figure 3(b) inset) [34].

The effects of dephasing γ_z and balanced spin flips $\gamma_\pm$ are shown in figure 3(b), where we compare the results of our protocol against time-reversed OAT, obtained by setting $\Omega = 0$ and $\delta = 3g_{\text{ion}}$ in equation (7). The results are similar to those of SnT: time-reversed OAT is somewhat more robust than our protocol at small γ_z for the considered system sizes, but fares worse in the presence of spin flips $\gamma_\pm$. Again using [32] as an example with $\gamma_\pm \approx 0.005g_{\text{ion}}$ and $\gamma_z \approx 0.05g_{\text{ion}}$, we find that our protocol is limited by γ_z and can provide

about 11 dB of metrological enhancement (see gray lines in figure 3(c)). By modifying the configuration of the ODF lasers, it should be possible to further reduce the effect of decoherence.

4. Cavity QED implementation

In cavity QED systems, the TC model (equation (1)) arises as the natural interaction between two-level atoms and an electromagnetic cavity mode. In the rotating frame of the atoms, the coupling between these degrees of freedom is described by

$$\hat{H}_{\text{TC}}^{\text{cav}} = -\Delta_{\text{cav}}\hat{a}^\dagger\hat{a} - ig_{\text{cav}}\left(\hat{a}\hat{S}^+ - \hat{a}^\dagger\hat{S}^-\right) \tag{11}$$

where Δ_{cav} is the detuning of the cavity with respect to the atomic transition frequency, $2g_{\text{cav}}$ is the single photon Rabi frequency, and $\hat{H}_{\text{TC}}$ (equation (1)) is recovered when $\Delta_{\text{cav}} = 0$. A direct comparison between equations (1) and (11) highlights a very important feature of cavity systems: the effective coupling constant G is N-dependent, i.e. $G_{\text{cav}} = g_{\text{cav}}\sqrt{N}$. For concreteness, we now consider the cavity implementation discussed in [20, 51], where ^{88}Sr atoms are trapped and cooled in a 1D optical lattice, and a high-finesse optical cavity is collectively coupled to the $^1S_0 \rightarrow {}^3P_1$ optical transition.

For the SnT protocol we set $\Delta_{\text{cav}} = 0$. The totally inverted initial spin state along $+z$ (see figure 1(b)) can be prepared by optical pumping (step (1)). Step (2) (application of $\hat{H}_{\text{TMS}}$ for a time T_{sq}) of the squeeze and transfer protocol then proceeds automatically because equation (11) is already of the TC form when $\Delta_{\text{cav}} = 0$. To perform the quench $\hat{H}_{\text{TC}} \rightarrow \hat{H}_{\text{ATC}}$, a rapid π pulse along x can be applied just before step (3), so that $\hat{S}^\pm \rightarrow \hat{S}^\mp$. We also note that no external drive is present during the entangling stage of the protocol (step (1)), in a similar spirit to other proposals [15]. The ideal (decoherence-free) scheme is limited only by finite size effects and follows the results for the ideal (decoherence-free) ion implementation (figure 2(a)). However, the cavity system is vulnerable to different sources of decoherence and technical noise, so we now focus on analyzing their impact on the achievable spin squeezing.

Relevant decoherence processes affecting the protocol come from leakage of photons through the cavity mirrors [36, 39–42] and spontaneous emission, modelled with respective jump operators $\sqrt{\kappa}\hat{a}$ and $\sqrt{\gamma}\hat{\sigma}_j^-$. The master equation that takes into account these effects, as well as the consequences of a finite π pulse duration, is
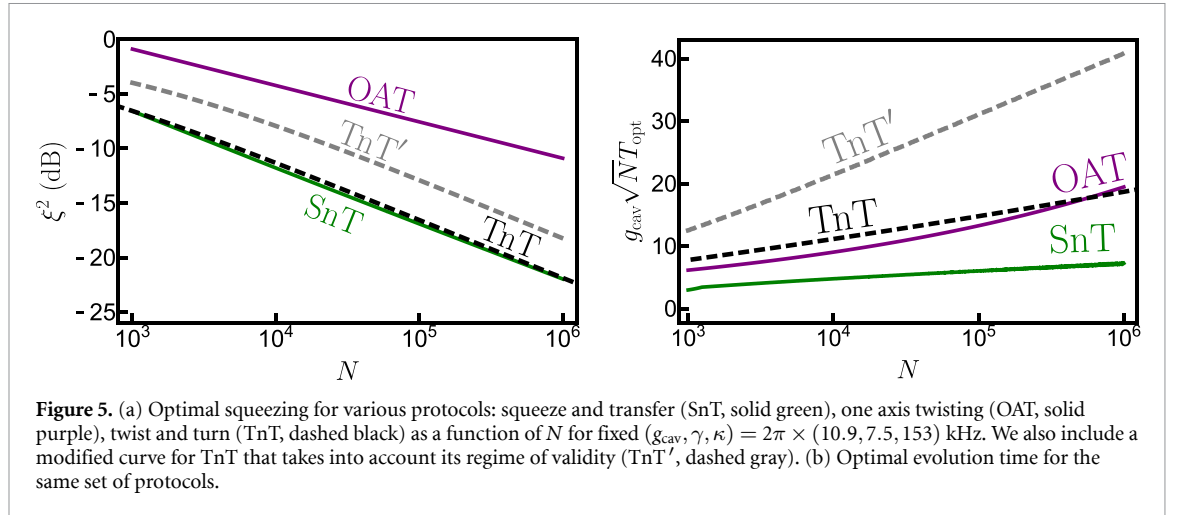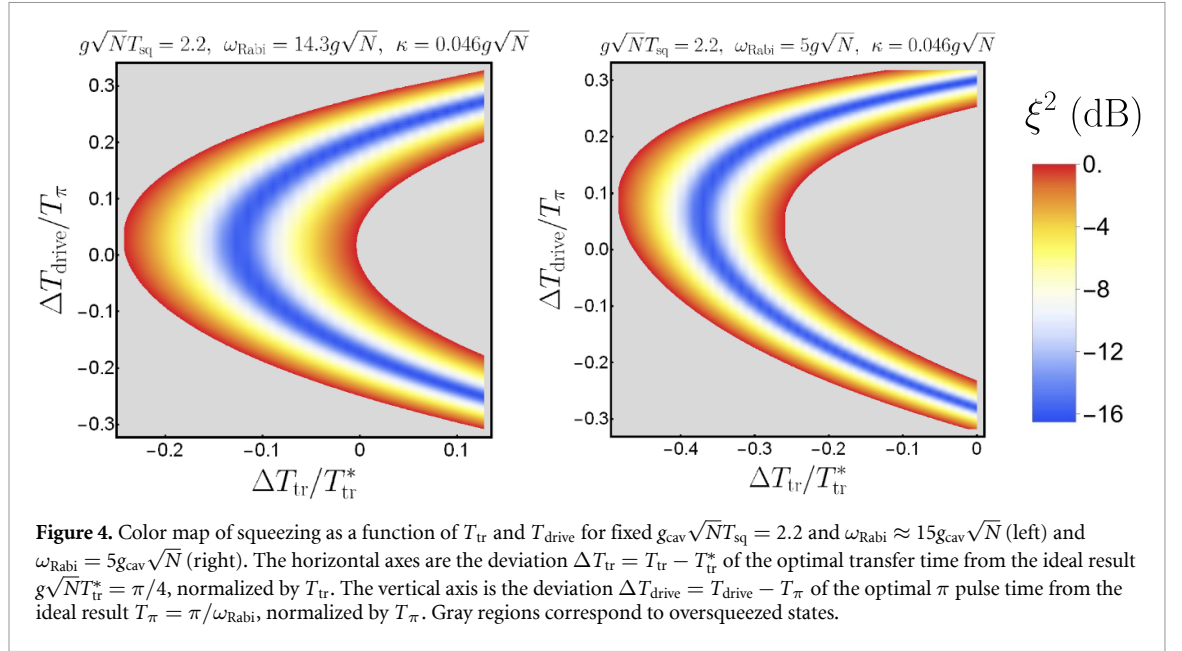
$$\partial_t\hat{\rho} = -i\left[g_{\text{cav}}\left(\hat{a}\hat{S}^+ + \hat{a}^\dagger\hat{S}^-\right) + \omega_{\text{Rabi}}(t)\hat{S}_y, \hat{\rho}\right]$$
$$+ \kappa\left(\hat{a}\hat{\rho}\hat{a}^\dagger - \frac{1}{2}\left\{\hat{a}^\dagger\hat{a}, \hat{\rho}\right\}\right) + \gamma\sum_{i=1}^{N}\left(\hat{\sigma}_i^-\hat{\rho}\hat{\sigma}_i^+ - \frac{1}{2}\left\{\hat{\sigma}_i^+\hat{\sigma}_i^-, \hat{\rho}\right\}\right), \tag{12}$$

where the Hamiltonian term $\omega_{\text{Rabi}}(t)\hat{S}_y$ models the π pulse.

We first consider the effects of the finite π pulse and assume $\gamma = 0$, which allows us to use the Holstein–Primakoff approximation to obtain analytic expressions [34]. The dynamics of the system can be subdivided into three stages—squeezing, π pulse, and transfer—that are characterized by the following time profile for $\omega_{\text{Rabi}}(t)$:

$$\omega_{\text{Rabi}}(t) = \begin{cases} 0, & 0 < t < T_{\text{sq}} & \text{Squeezing (duration } T_{\text{sq}}) \\ \omega_{\text{Rabi}}, & T_{\text{sq}} < t < T_{\text{sq}} + T_{\text{drive}} & \pi \text{ pulse (duration } T_{\text{drive}}) \\ 0, & T_{\text{sq}} + T_{\text{drive}} < t < T_{\text{sq}} + T_{\text{drive}} + T_{\text{tr}} & \text{Transfer (duration } T_{\text{tr}}). \end{cases} \tag{13}$$

Under ideal conditions the Rabi pulse is instantaneous, i.e. $\omega_{\text{Rabi}} \gg g_{\text{cav}}\sqrt{N}$, in which case $T_{\text{drive}} \approx \pi/\omega_{\text{Rabi}} \equiv T_\pi$ and $T_{\text{tr}} \approx \pi/(4g_{\text{cav}}\sqrt{N}) \equiv T_{\text{tr}}^*$, where T_π and T_{tr}^* are the ideal Rabi pulse and transfer times, respectively. However, when ω_{drive} is finite compared to $g_{\text{cav}}\sqrt{N}$, the atom-light dynamics in the cavity can impact the quality of the π pulse, reducing the amount of spin squeezing obtained at the end of the protocol. This can be mitigated by modifying T_{drive} and T_{tr} with respect to the ideal values T_π and T_{tr}^*. This is shown in figure 4, where the final spin squeezing is plotted as a function of $\Delta T_{\text{drive}} = T_{\text{drive}} - T_\pi$ and $\Delta T_{\text{tr}} = T_{\text{tr}} - T_{\text{tr}}^*$ for two values of $\omega_{\text{Rabi}}/(g_{\text{cav}}\sqrt{N}) = 14.3, 5$ and fixed $g_{\text{cav}}\sqrt{N}T_{\text{sq}} = 2.2$, $\kappa = 0.046g_{\text{cav}}\sqrt{N}$. Even for ω_{Rabi} as low as $5g_{\text{cav}}\sqrt{N}$, a large amount of squeezing can be recovered by appropriately modifying T_{drive} and T_{sq}. Physically, this is the result of photons being coherently emitted into the cavity via the TC interaction as the spins are rotated from $+z$ to $-z$, which can then induce additional rotation of the Bloch vector and corresponding noise profile. This modifies the optimal duration of the π pulse and transfer steps.

Figure 4. Color map of squeezing as a function of T_{tr} and T_{drive} for fixed $g_{\mathrm{cav}}\sqrt{N}T_{\mathrm{sq}} = 2.2$ and $\omega_{\mathrm{Rabi}} \approx 15 g_{\mathrm{cav}}\sqrt{N}$ (left) and $\omega_{\mathrm{Rabi}} = 5 g_{\mathrm{cav}}\sqrt{N}$ (right). The horizontal axes are the deviation $\Delta T_{\mathrm{tr}} = T_{\mathrm{tr}} - T_{\mathrm{tr}}^*$ of the optimal transfer time from the ideal result $g\sqrt{N}T_{\mathrm{tr}}^* = \pi/4$, normalized by T_{tr}. The vertical axis is the deviation $\Delta T_{\mathrm{drive}} = T_{\mathrm{drive}} - T_\pi$ of the optimal π pulse time from the ideal result $T_\pi = \pi/\omega_{\mathrm{Rabi}}$, normalized by T_π. Gray regions correspond to oversqueezed states.

Figure 5. (a) Optimal squeezing for various protocols: squeeze and transfer (SnT, solid green), one axis twisting (OAT, solid purple), twist and turn (TnT, dashed black) as a function of N for fixed $(g_{\mathrm{cav}}, \gamma, \kappa) = 2\pi \times (10.9, 7.5, 153)$ kHz. We also include a modified curve for TnT that takes into account its regime of validity (TnT$'$, dashed gray). (b) Optimal evolution time for the same set of protocols.

We now analyze the effect of a finite γ, assuming an instantaneous π pulse for simplicity. Because of the single particle nature of spontaneous emission we can no longer use the Holstein–Primakoff approximation. However, the large N approximation can still be implemented directly on the equations of motion. This is done by first solving the mean field dynamics, and then computing the fluctuations about these mean field values [34], which are generically smaller by a factor of $\sqrt{N}$. The achievable squeezing depends independently on both κ/g_{cav}, γ/g_{cav}, so we keep these fixed and compute the squeezing parameter as a function of N after optimization over T_{tr} and T_{sq}. We use the values $(g_{\mathrm{cav}}, \gamma, \kappa) = 2\pi \times (10.9, 7.5, 153)$ kHz [20, 51], and vary N in the range $(10^3, 10^6)$. The results are shown in figure 5(a), which indicate that the optimal squeezing scales as $N^{-1/2}$.

It is possible to obtain analytical formulas when $\kappa \gg \gamma$. Then the achievable spin squeezing is [34]

$$\xi_{\mathrm{opt}}^2 = \frac{\pi\kappa}{8 g_{\mathrm{cav}}\sqrt{N}} \approx \frac{0.4\kappa}{g_{\mathrm{cav}}\sqrt{N}}, \tag{14}$$

obtained at $g_{\mathrm{cav}}\sqrt{N}T_{\mathrm{tr}} = \pi/4 + \kappa/(4 g_{\mathrm{cav}}\sqrt{N})$ and $2 g_{\mathrm{cav}}\sqrt{N}T_{\mathrm{sq}} \gtrsim \log\left(2.5 g_{\mathrm{cav}}\sqrt{N}/\kappa\right)$. This calculation is consistent with the $N^{-1/2}$ scaling of the optimal squeezing and optimal protocol time (up to logarithmic corrections) that we observe in the numerical simulations shown in figure 5. For $N \approx 10^5$ particles, 15 dB of squeezing are attainable. Equation (14) also indicates that this N dependence comes from the scaling of $G_{\mathrm{cav}} = g_{\mathrm{cav}}\sqrt{N}$ and is not a consequence of curvature effects, which we expect to be irrelevant for the number of atoms that can be typically loaded into these cavity setups.

Finally, we also compare SnT against OAT and twist-and-turn (TnT) [17] protocols, both of which can be engineered by operating the cavity in a far-detuned regime $|\Delta_{\text{cav}}| \gg g_{\text{cav}}\sqrt{N}$ [15]:

$$\hat{H}_{\text{OAT}}^{\text{cav}} = \chi_{\text{cav}}\hat{S}_z^2, \qquad \hat{H}_{\text{TnT}}^{\text{cav}} = \chi_{\text{cav}}\left(\hat{S}_z^2 + \hat{S}_x\right), \qquad (15)$$

where $\chi_{\text{cav}} = 4g^2\Delta_{\text{cav}}/(4\Delta_{\text{cav}}^2 + \kappa^2)$. In the presence of the same decoherence sources considered in SnT, optimization of squeezing over $\Delta_{\text{cav}}/\kappa$ and evolution time leads to $\xi_{\text{OAT}}^2 = 6(CN)^{-1/3}$ [15, 52] and $\xi_{\text{TnT}}^2 \approx 4.6(CN)^{-1/2}$ [15, 34], where $C = 4g_{\text{cav}}^2/(\kappa\gamma)$ is the cooperativity parameter. These results are also shown in figure 5(a) as a function of N for the same values of $g_{\text{cav}}, \gamma, \kappa$ as for SnT. However, with this set of parameters the optimal detuning for TnT satisfies $\Delta_{\text{cav}}^{\text{opt}} \approx 2.5g_{\text{cav}}\sqrt{N}$, which is beyond the regime of validity for $\hat{H}_{\text{TnT}}^{\text{cav}}$ in equation (15). If we instead fix $\Delta_{\text{cav}} = 10g_{\text{cav}}\sqrt{N}$ to guarantee the applicability of equation (15) and optimize over evolution time, we obtain results denoted by the gray line labelled TnT′ in figure 5. For completeness, in figure 5(b) we show the total protocol times, measured in units of $(g_{\text{cav}}\sqrt{N})^{-1}$, as a function of N, and note that SnT yields the shortest protocol time.

5. Outlook

We have discussed protocols that take full advantage of the resonant spin-boson coupling and yield exponentially fast generation of squeezing, which can mitigate the impact of decoherence. These protocols are relevant for a range of spin-boson platforms at the cutting edge of quantum sensing applications. Although we only examine deterministic protocols, an interesting future direction would be the investigation of how dynamical evolution combined with non-demolition measurements can lead to further improvement.

Data availability statement

All data that support the findings of this study are included within the article (and any supplementary files).

Acknowledgments

ORCID iDs

Diego Barberena ⓘ https://orcid.org/0000-0002-6845-1807
Sean R Muleady ⓘ https://orcid.org/0000-0002-5005-3763
John J Bollinger ⓘ https://orcid.org/0000-0001-9117-7896
Robert J Lewis-Swan ⓘ https://orcid.org/0000-0002-0201-281X
Ana Maria Rey ⓘ https://orcid.org/0000-0001-7176-9413

References

[1] Kitagawa M and Ueda M 1993 Squeezed spin states *Phys. Rev.* A **47** 5138–43
[2] Ma J, Wang X, Sun C and Nori F 2011 Quantum spin squeezing *Phys. Rep.* **509** 89–165
[3] Degen C L, Reinhard F and Cappellaro P 2017 Quantum sensing *Rev. Mod. Phys.* **89** 035002
[4] Caves C M, Thorne K S, Drever R W P, Sandberg V D and Zimmermann M 1980 On the measurement of a weak classical force coupled to a quantum-mechanical oscillator. I. Issues of principle *Rev. Mod. Phys.* **52** 341–92
[5] Cox K C, Greve G P, Weiner J M and Thompson J K 2016 Deterministic squeezed states with collective measurements and feedback *Phys. Rev. Lett.* **116** 093602
[6] Hosten O, Engelsen N J, Krishnakumar R and Kasevich M A 2016 Measurement noise 100 times lower than the quantum-projection limit using entangled atoms *Nature* **529** 505–8
[7] Pedrozo-Peñafiel E *et al* 2020 Entanglement on an optical atomic-clock transition *Nature* **588** 414–8
[8] Muessel W, Strobel H, Linnemann D, Hume D B and Oberthaler M K 2014 Scalable spin squeezing for quantum-enhanced magnetometry with Bose–Einstein condensates *Phys. Rev. Lett.* **113** 103004
[9] Hosten O, Krishnakumar R, Engelsen N J and Kasevich M A 2016 Quantum phase magnification *Science* **352** 1552–5
[10] Schleier-Smith M H, Leroux I D and Vuletić V 2010 States of an ensemble of two-level atoms with reduced quantum uncertainty *Phys. Rev. Lett.* **104** 073604
[11] Leroux I D, Schleier-Smith M H and Vuletić V 2010 Implementation of cavity squeezing of a collective atomic spin *Phys. Rev. Lett.* **104** 073602

[12] Bohnet J G, Sawyer B C, Britton J W, Wall M L, Rey A M, Foss-Feig M and Bollinger J J 2016 Quantum spin dynamics and entanglement generation with hundreds of trapped ions *Science* **352** 1297–301

[13] Pezzè L, Smerzi A, Oberthaler M K, Schmied R and Treutlein P 2018 Quantum metrology with nonclassical states of atomic ensembles *Rev. Mod. Phys.* **90** 035005

[14] Qin W, Chen Y-H, Wang X, Miranowicz A and Nori F 2020 Strong spin squeezing induced by weak squeezing of light inside a cavity *Nanophotonics* **9** 4853–68

[15] Hu J, Chen W, Vendeiro Z, Urvoy A, Braverman B and Vuletić V 2017 Vacuum spin squeezing *Phys. Rev.* A **96** 050301(R)

[16] Borregaard J, Davis E J, Bentsen G S, Schleier-Smith M H and Sørensen A S 2017 One- and two-axis squeezing of atomic ensembles in optical cavities *New J. Phys.* **19** 093021

[17] Muessel W, Strobel H, Linnemann D, Zibold T, Juliá-Díaz B and Oberthaler M K 2015 Twist-and-turn spin squeezing in bose-einstein condensates *Phys. Rev.* A **92** 023603

[18] Holland M J and Burnett K 1993 Interferometric detection of optical phase shifts at the heisenberg limit *Phys. Rev. Lett.* **71** 1355–8

[19] Zurek W H 2001 Sub-Planck structure in phase space and its relevance for quantum decoherence *Nature* **412** 712–7

[20] Norcia M A and Thompson J K 2016 Strong coupling on a forbidden transition in strontium and nondestructive atom counting *Phys. Rev.* A **93** 023804

[21] Tavis M and Cummings F W 1968 Exact solution for an *n*-molecule—radiation-field hamiltonian *Phys. Rev.* **170** 379–84

[22] Holstein T and Primakoff H 1940 Field dependence of the intrinsic domain magnetization of a ferromagnet *Phys. Rev.* **58** 1098–113

[23] Wineland D J, Bollinger J J, Itano W M, Moore F L and Heinzen D J 1992 Spin squeezing and reduced quantum noise in spectroscopy *Phys. Rev.* A **46** R6797–800

[24] Gerry C and Knight P 2004 Nonclassical light *Introductory Quantum Optics* (Cambridge University Press) pp 150–94

[25] Yurke B, McCall S L and Klauder J R 1986 SU(2) and SU(1,1) interferometers *Phys. Rev.* A **33** 4033–54

[26] Penasa M, Gerlich S, Rybarczyk T, Métillon V, Brune M, Raimond J M, Haroche S, Davidovich L and Dotsenko I 2016 Measurement of a microwave field amplitude beyond the standard quantum limit *Phys. Rev.* A **94** 022313

[27] Burd S C, Srinivas R, Bollinger J J, Wilson A C, Wineland D J, Leibfried D, Slichter D H and Allcock D T C 2019 Quantum amplification of mechanical oscillator motion *Science* **364** 1163–5

[28] Linnemann D, Strobel H, Muessel W, Schulz J, Lewis-Swan R J, Kheruntsyan K V and Oberthaler M K 2016 Quantum-enhanced sensing based on time reversal of nonlinear dynamics *Phys. Rev. Lett.* **117** 013001

[29] Davis E, Bentsen G and Schleier-Smith M 2016 Approaching the heisenberg limit without single-particle detection *Phys. Rev. Lett.* **116** 053601

[30] Macrì T, Smerzi A and Pezzè L 2016 Loschmidt echo for quantum metrology *Phys. Rev.* A **94** 010102

[31] Colombo S, Pedrozo-Peñafiel E, Adiyatullin A F, Li Z, Mendez E, Shu C and Vuletic V 2022 Time-reversal-based quantum metrology with many-body entangled states *Nat. Phys.* **18** 925–30

[32] Gilmore K A, Affolter M, Lewis-Swan R J, Barberena D, Jordan E, Rey A M and Bollinger J J 2021 Quantum-enhanced sensing of displacements and electric fields with two-dimensional trapped-ion crystals *Science* **373** 673–8

[33] Li Z, Colombo S, Shu C, Velez G, Pilatowsky-Cameo S, Schmied R, Choi S, Lukin M, Pedrozo-Peñafiel E and Vuletić V 2023 Improving metrology with quantum scrambling *Science* **380** 1381–4

[34] See supplemental material at [URL will be inserted by publisher]

[35] Dicke R H 1954 Coherence in spontaneous radiation processes *Phys. Rev.* **93** 99–110

[36] Baumann K, Guerlin C, Brennecke F and Esslinger T 2010 Dicke quantum phase transition with a superfluid gas in an optical cavity *Nature* **464** 1301–6

[37] Lewis-Swan R, Safavi-Naini A, Bollinger J J and Rey A M 2019 Unifying scrambling, thermalization and entanglement through measurement of fidelity out-of-time-order correlators in the Dicke model *Nat. Commun.* **10** 1–9

[38] Safavi-Naini A, Lewis-Swan R J, Bohnet J G, Gärttner M, Gilmore K A, Jordan J E, Cohn J, Freericks J K, Rey A M and Bollinger J J 2018 Verification of a many-ion simulator of the Dicke model through slow quenches across a phase transition *Phys. Rev. Lett.* **121** 040503

[39] Kirton P, Roses M M, Keeling J and Dalla Torre E G 2019 Introduction to the Dicke model: from equilibrium to nonequilibrium and vice versa *Adv. Quantum Technol.* **2** 1800043

[40] Zhiqiang Z, Lee C H, Kumar R, Arnold K J, Masson S J, Parkins A S and Barrett M D 2017 Nonequilibrium phase transition in a spin-1 Dicke model *Optica* **4** 424–9

[41] Kroeze R M, Guo Y, Vaidya V D, Keeling J and Lev B L 2018 Spinor self-ordering of a quantum gas in a cavity *Phys. Rev. Lett.* **121** 163601

[42] Klinder J, Keßler H, Wolke M, Mathey L and Hemmerich A 2015 Dynamical phase transition in the open Dicke model *Proc. Natl Acad. Sci.* **112** 3290–5

[43] Safavi-Naini A, Lewis-Swan R J, Bohnet J G, Garttner M, Gilmore K A, Jordan E, Cohn J, Freericks J K, Rey A M and Bollinger J J 2017 Exploring adiabatic quantum dynamics of the Dicke model in a trapped ion quantum simulator (arXiv:1711.07392)

[44] Strobel H, Muessel W, Linnemann D, Zibold T, Hume D B, Pezze L, Smerzi A and Oberthaler M K 2014 Fisher information and entanglement of non-Gaussian spin states *Science* **345** 424–7

[45] Baamara Y, Sinatra A and Gessner M 2021 Scaling laws for the sensitivity enhancement of non-Gaussian spin states *Phys. Rev. Lett.* **127** 160501

[46] Huelga S F, Macchiavello C, Pellizzari T, Ekert A K, Plenio M B and Cirac J I 1997 Improvement of frequency standards with quantum entanglement *Phys. Rev. Lett.* **79** 3865–8

[47] Escher B M, de Matos Filho R L and Davidovich L 2011 General framework for estimating the ultimate precision limit in noisy quantum-enhanced metrology *Nat. Phys.* **7** 406–11

[48] Wall M L, Safavi-Naini A and Rey A M 2017 Boson-mediated quantum spin simulators in transverse fields: *XY* model and spin-boson entanglement *Phys. Rev.* A **95** 013602

[49] Huber J, Rey A M and Rabl P 2022 Realistic simulations of spin squeezing and cooperative coupling effects in large ensembles of interacting two-level systems *Phys. Rev.* A **105** 013716

[50] Carter A L, Muleady S R, Shankar A, Lilieholm J F, Bullock B B, Affolter M, Rey A M and Bollinger J J 2023 Comparison of spontaneous emission in trapped ion multi-qubit gates at high magnetic fields *Phys. Rev.* A **107** 042618

[51] Muniz J A, Barberena D, Lewis-Swan R J, Young D J, Cline J R K, Rey A M and Thompson J K 2020 Exploring dynamical phase transitions with cold atoms in an optical cavity *Nature* **580** 602–7

[52] Lewis-Swan R J, Norcia M A, Cline J R K, Thompson J K and Rey A M 2018 Robust spin squeezing via photon-mediated interactions on an optical clock transition *Phys. Rev. Lett.* **121** 070403